Plasma turbulence of nonspecular trail plasmas as measured by a high-power large-aperture radar

Jonathan Yee[1] and Sigrid Close[1]

[1]   High-power, large-aperture radars have been used to characterize plasmas formed as meteoroids ablate in Earth's atmosphere. These plasmas are referred to as heads, the plasmas surrounding the meteoroids, and trails, the plasmas left behind by the meteoroids. A subset of trails is nonspecular trails, which are detected when the radar beam is quasi-perpendicular to the magnetic field. Radar returns from trail plasma are thought to originate from field-aligned irregularity reflections that form due to turbulence within the trail. In this paper, we present theory and analysis of plasma trail diffusion using nonspecular trails detected by the Advanced Research Project Agency Long-range Tracking and Identification Radar. These data include dual frequency, dual polarized, and high-range resolution in-phase and quadrature returns with azimuth and elevation data. We present turbulence onset times for nonspecular trails and derive comparisons to models. We compare diffusion coefficients calculated from the decay in signal return with ambipolar diffusion coefficients derived for specular meteor trails. These results, in conjunction with an analysis of the diffusion perpendicular and parallel to the magnetic field, demonstrate that the ambipolar diffusion coefficient is not a sufficient description of the turbulent diffusion in nonspecular trails and that other influences, such as external electric fields and anomalous cross-field diffusion, must be considered when calculating the diffusion coefficients of nonspecular trails. In addition, we examined these results with respect to the polarization of the returns and found similar trends between all polarizations with slight differences for the right circular return.

1.   Introduction

[2]   As meteoroids enter Earth's atmosphere at velocities greater than 10 km/s, they begin to heat up and ablate atoms due to the interaction between the meteoroids and the atmosphere. These ablating atoms subsequently collide with neutral air molecules and form columns of partially ionized plasma between altitudes of 70 and 140 km. High-power large-aperture (HPLA) radars detect the signatures from the plasma formed by the meteoroid, known as a meteor. These observations of meteors in the *E* region of the ionosphere are important in understanding the development and evolution of plasmas in a collisional environment. Not only can we study the plasma from the meteors but we can also derive ambient ionosphere conditions. For example, *Oppenheim et al.* [2009] developed a technique by which nonspecular meteor trails could be used to compute neutral wind measurements by comparing the phase differences between detection channels from the Jicamarca Radio Observatory [*Oppenheim et al.*, 2009]. With these measurements, *Oppenheim et al.* [2009] was able to discuss the influence of these neutral winds on the bulk fluid motion of the meteor trails in the ionosphere. In addition to helping with the prediction and understanding of neutral winds and other atmospheric phenomena, meteor research provides insight into understanding space plasmas including plasmas that are generated from meteoroid impacts on satellites [*Close et al.*, 2010; *Lee et al.*, 2012].

[3]   Collisional environment meteor studies have focused on head echoes, specular trails, and nonspecular trails that are left in the wake of a meteoroid. Head echoes are the return from the plasma generated directly around the meteoroid as it enters the atmosphere. The head echo generally travels with the velocity of the meteoroid and is the closest of the three to a point target reflection. Specular trails occur when the radar beam is approximately pointed perpendicular to the meteoroid's path and arise from Fresnel scattering from the meteor. Specular trails tend to have strong signal returns; consequently, past studies of specular trails have been done with low-power radars and instrumentation [*Sugar*, 1964; *Chilson et al.*, 1996; *Hocking et al.*, 2000; *Galligan et al.*, 2004; *Hall et al.*, 2005; *Ballinger et al.*, 2008; *Kumar and Subrahmanyam*, 2012]. In recent years, HPLA radars have become the primary tool for characterizing and studying

[1]Aeronautics and Astronautics Department, Stanford University, Stanford, California, USA.

Corresponding author: J. Yee, Aeronautics and Astronautics Department, Stanford University, 496 Lomita Mall, Stanford, CA 94305, USA. (jcyee@stanford.edu)

Table 1. Summary of UHF and VHF Data Collection Parameters[a]

Parameter	VHF (V7100)	UHF (U5400)
T (μs)	100	400
f_0 (MHz)	158	422
B (MHz)	7.06	5.00
PRF (Hz)	115	115

[a]T is the pulsewidth, f_0 is the radar radio frequency, B is the bandwidth, and PRF is the pulse repetition frequency.

meteor trails [*Chau et al.*, 2007; *Close et al.*, 2008, 2011]. These more powerful radars have allowed for the detection of nonspecular trails traveling quasi-parallel to the beam, which are not normally detected by low-power radars. These nonspecular trails, which result from the same plasma detected in specular trails but through a different viewing geometry, are generally detected when the HPLA radar beam is pointed quasi-perpendicular to the background magnetic field [*Close et al.*, 2008]. These detections are thought to be the reflection from the Bragg scattering of electrons from a final turbulent stage within the plasma as it forms field-aligned irregularities [*Heritage et al.*, 1962]. An important distinction between specular and nonspecular trail studies is that each specular trail is confined within a much narrower altitude extent than nonspecular trails; studies that develop altitude dependence of trail diffusion coefficients based on specular trails must be based on a large amount of detections. This requirement of detections of multiple specular trails to study a large range of altitudes could lead to errors when exploring the relationship between meteor diffusion coefficients and altitude due to differences in meteoroid mass, composition, velocity, and ambient conditions. In contrast, a single nonspecular trail spans a large range of altitudes, thereby allowing for the study of diffusive properties without changing the "input function". Additionally, other aspects of the plasma turbulence can be examined, such as the development time between head echo and trail formation.

[4] In this paper, we present an analysis of a set of 152 nonspecular trails detected at 160 MHz and 422 MHz with the Advanced Research Project Agency Long-range Tracking and Identification Radar (ALTAIR). Trails were detected in both left-circularly polarized (LC) and right-circularly polarized (RC) wave returns, which can be combined for the total polarized wave return. In addition, traverse (TR) and elevation (EL) monopulse angles were measured for all detected nonspecular trails. These high-resolution, polarized data were used to calculate turbulence onset times and diffusion coefficients, which were subsequently compared to previous studies [*Jones and Jones*, 1990; *Galligan et al.*, 2004]. Additionally, we examined diffusion of particles perpendicular and parallel to the magnetic field lines for the detected nonspecular trails over the course of the trail's lifetime. Section 1 describes the instrumentation and observations. Section 2 reports and compares the averaged turbulence onset times to nonspecular trail models. Section 3 describes calculated values for the diffusion coefficients and compares these to ambipolar diffusion coefficients measured at other radars detecting specular trails. Section 4 describes the evolution of the nonspecular trails and compares the diffusion of particles perpendicular and parallel to the magnetic field lines. Section 5 summarizes and concludes our findings.

1.1. Instrumentation

[5] ALTAIR is a 46 m diameter HPLA radar located on the Kwajalein Atoll of the Marshall Islands in the Pacific Ocean. It operates with dual frequency at Ultra High Frequency (UHF) and Very High Frequency (VHF), 422 MHz and 160 MHz, respectively. ALTAIR transmits a RC signal at a peak power of 6 MW in a half-power beam width of 2.8° (VHF) and 1.1° (UHF). In addition to receiving both LC and RC energy in the main receiving horn, ALTAIR uses a combination of five receiving horns, the main receiving horn plus four additional receiving horns, to measure both TR and EL angles; TR is converted to azimuth (AZ) by using the radar boresite angle. When these measurements are used in combination with the measured range, three-dimensional (3-D) position, velocity, and deceleration of detected objects can be determined. ALTAIR is actively calibrated by the tracking of standard calibration spheres for both signature and metric data. These spheres trace out the ALTAIR beam pattern for both LC and RC signals as a function of position within the beam in order to attempt to eliminate polarized returns that depend on beam position. In total, ALTAIR provides the in-phase (I) and quadrature (Q) components for LC, RC, TR, and EL in both VHF and UHF.

1.2. Observations

[6] Approximately 30 h of radar meteor data were collected at ALTAIR during 2007 and 2008. During the year-long collection period, sporadic meteor data were collected at both VHF and UHF typically around 1800 UTC (6 A.M. local time). Amplitude and phase data were recorded for each frequency for altitudes spanning 80 to 140 km. Two linear frequency modulated waveforms, "V7100" and "U5400", chosen for their high-sensitivity and high-range resolution, were used to collect the data. V7100 was a 100 μs pulse width VHF chirped pulse with 15 m range spacing, while U5400 was a 400 μs pulse width UHF chirped pulse also with 15 m range spacing. Due to ALTAIR system requirements, a 115 Hz pulse repetition frequency (PRF) was employed with these two waveforms. These ALTAIR waveform parameters are summarized in Table 1.

[7] We found 152 nonspecular trails with signal-to-noise ratio (SNR) higher than 15 dB that were also unobstructed by radar detection of background ionospheric phenomena. The 152 trails correspond to sporadic meteoroids with

Table 2. Summary of the VHF, UHF, LC, RC, and Total Detections[a]

			Simultaneous Detections					
			UHF			VHF		
Frequency	Polarization	Detections	LC	RC	Total	LC	RC	Total
VHF	LC	109	23	5	23	-	67	109
	RC	67	19	5	19	67	-	67
	Total	109	23	5	23	109	67	-
UHF	LC	43	-	5	43			
	RC	5	5	-	5			
	Total	43	43	5	-			

[a]VHF and UHF detections for LC, RC, and total return on the left side. The right side summarizes the simultaneous detections between all the combinations of LC, RC, Total, VHF, and UHF detections.

ALTAIR boresite-pointing angles spanning up to 10° off of perpendicular with respect to the background magnetic field. All 152 trails had head echo and nonspecular trail detections in the LC channel, but only 72 of the 152 trails had corresponding RC channel head echo and nonspecular trail detections. Additionally, of the 43 UHF and 109 VHF nonspecular trails that were analyzed, only 23 trails in the LC channel and 5 trails in the RC channel had concurrent detections without background interference at UHF and VHF. The number of LC, RC, Total, VHF, UHF, and simultaneous detections are summarized in Table 2. Figure 1 shows an example of two of the 152 nonspecular trails and their head echoes detected at both LC and RC return and UHF and VHF simultaneously.

2. Turbulence Onset

[8] Modeling of nonspecular trail formation has been an active research area with focus on explaining and predicting how nonspecular meteor trails form and diffuse. The first such models were developed and reported nearly a decade ago [*Oppenheim et al.*, 2000; *Dyrud et al.*, 2001], with further simulation results and comparisons being presented periodically throughout the last decade [*Dyrud et al.*, 2002; *Oppenheim et al.*, 2003a; *Oppenheim et al.*, 2003b; *Dyrud et al.*, 2007]. These models argue that after the head echo has passed through a region, the formation of radar-detectable nonspecular trails follows a several step process. First, as soon as the trail begins formation, an electric field forms within the quasineutral plasma. Gradient-drift/Farley Buneman (GDFB)

waves then begin to form along the edges of the electric field. Due to the strong electric field within the plasma and the steep gradients at the edges, the GDFB instabilities continue to develop. Eventually, the instabilities become unstable and turbulence sets in within the plasma. As a result of this turbulence, field-aligned density irregularities develop which are subsequently detected by radars; an example is shown in Figure 1. However, this process does not occur instantaneously. Instead, after the formation of the head echo, there is a delay before the detection of a nonspecular trail and the onset of turbulence. It is possible that these turbulence onset times might be able to help in predicting parent meteoroid properties or indicate ambient atmospheric conditions at the time of detection, since some simulations have suggested a dependence of turbulence onset times on background conditions [*Oppenheim et al.*, 2000; *Oppenheim et al.*, 2003a; *Oppenheim et al.*, 2003b]. Altogether, multiple simulations and previous meteor radar data have shown that these onset times, depending on the ambient conditions, can vary anywhere from 20 to 40 ms [*Close et al*, 2002].

2.1. Measuring Turbulence Onset From Radar Signals

[9] In order to measure the time for the turbulence to set in within the meteor trail, we first calculated the range and time of the head echo for all ALTAIR detections. Since the head echo detection altitudes primarily follow a linear relationship with time, we fit a line to the head echo path, as shown by the green streak over the head echo in Figure 2. Next we located the nonspecular trail by finding a set of three consecutive
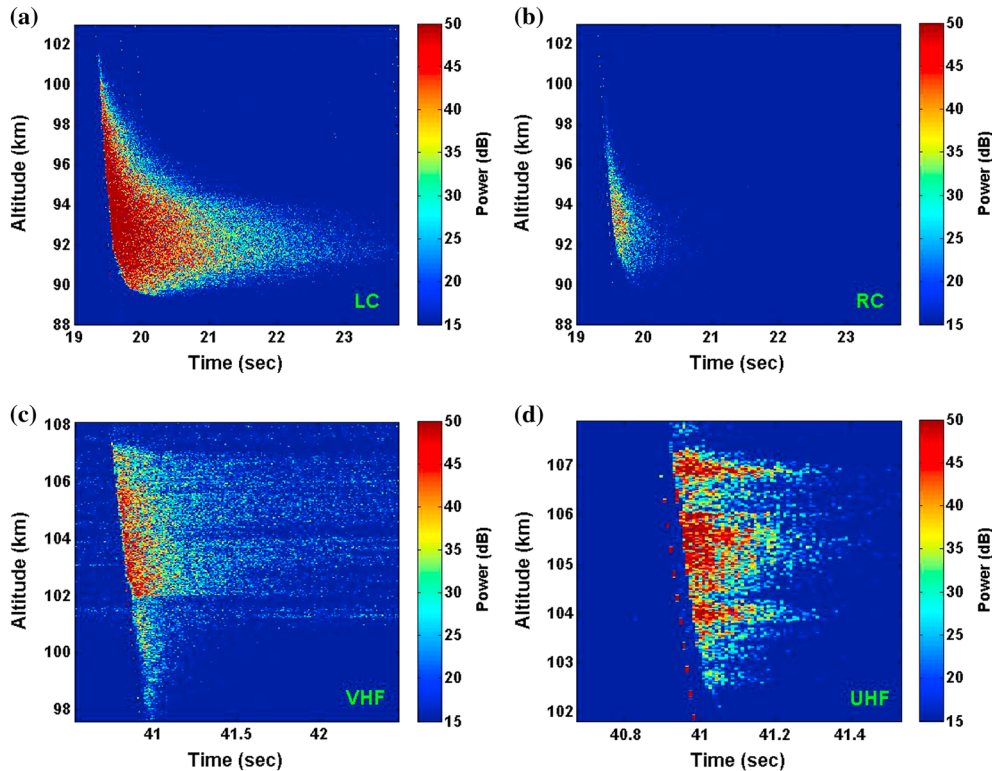

Figure 1. Examples of signal return from nonspecular trails plotted for altitude verse time color coded for power return. The first two returns are simultaneous detections in the (a) LC and (b) RC channels of the same trail from 18 November 2007. The latter two returns are detections from a second trail simultaneously detected in the (c) VHF and (d) UHF channels on 6 January 2007.
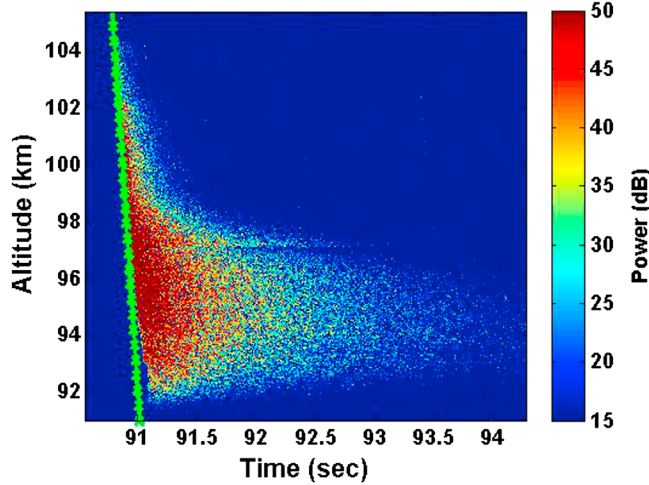
Figure 2. Nonspecular trail example with a line (green crosses) fitted to the head echo position with time. Trail data example is from 2 January 2007.

radar returns that were larger than 15 dB. The first of these three points were identified as the start of the nonspecular trail. A last step before finding the onset times was to shift the head echo time location by the range-Doppler coupling constant. This range-Doppler coupling is a property of a chirp-type pulse and causes a shift in apparent range determined by equation (1).

$$\Delta r = \frac{T \times f_0}{B} v_r \qquad (1)$$

where Δr is the range offset, T is the pulsewidth, f_0 is the radar transmitted frequency, v_r is the target radial velocity, and B is the chirp bandwidth. Note, if we divide both sides by the radial velocity, the left-hand side simply becomes the time shift constant due to the range-Doppler coupling. The time shift constant for the head echo can be calculated from the values in Table 1, both for UHF (3.38×10^{-2} s) and VHF (2.20×10^{-3} s). Once the head echo was shifted, as shown in the example in Figure 3, we then found the difference between the head echo detection time, as predicted by the shifted fit for the given head echo, and the nonspecular trail start detection time for each altitude bin.

2.2. Turbulence Onset of Nonspecular Trails

[10] The process described in section 2.1 was followed for each of the 152 trails analyzed in this study. We calculated turbulence onset times for each trail at a measured altitude bin. These altitudes were rounded to the nearest integer altitude, and the trail's onset times were averaged for each of these rounded altitudes. We then averaged over all 152 of these individual trails, regardless of signal return type, and plotted these onset times as a function of altitudes in Figure 4a. In addition, we divided the onset times based on signal return type (i.e., LC, RC, or total) and frequency (i.e., UHF and VHF) and plotted these results in Figures 4b–4d. Additionally, 25 and 45 ms lines are included on the plots in cyan and black, respectively, for comparison with the data results.

[11] As seen in all four cases, the turbulence onset times show slight fluctuations but tend to remain within the 25 and 40 ms delay lines until an altitude of approximately 95 km with the exception of the RC return. At these lower altitudes, the onset times sharply increase with decreasing altitude to the order of 10^{-1} s. This sharp increase was predicted in previously reported nonspecular trail models [*Oppenheim et al.*, 2000; *Dyrud et al.*, 2005] and was caused by the inclusion of a background electric field or a neutral wind in the ambipolar electric field present within the trail. These background influences included the ion collision frequency and the peak density, which both increase at lower altitudes and are thought to be a part of the reason for the increase in onset times. Examining the breakdown by signal return, we see that the LC onset delays clearly have fewer fluctuations than RC onset delays, especially below 102 km altitude. Interestingly, when the time delays are broken down by frequency, the same patterns remain with the RC return still having far more fluctuations than the LC time delays. This difference is most likely due to the lower SNR returns in RC than in LC which can result in sparser trail detections and inconsistences in determining the initial trail detection. However, the sharp increase with decreasing altitude seems to occur twice for the UHF RC return at 103 and 95 km rather than just once below altitudes of 95 km. Other differences arise as we continue to examine the UHF and VHF trails. The VHF average seems to have a more gradual increase in time delay as the altitude decreases below 97 km, whereas the UHF average stays between 25 and 40 ms before suddenly increasing to larger values around 95 km. However, despite these differences, most of the results between the VHF and UHF time delays remain below the predicted 40 ms. These differences within the onset time breakdowns are most likely explained by the lack of return data at lower altitudes for the UHF or RC return. However, this remains an unexplained phenomenon that is left for future work.

3. Ambipolar Diffusion Coefficient

[12] Traditionally, meteor trail studies have assumed that the formed plasma column is a singly, weakly ionized plasma in a
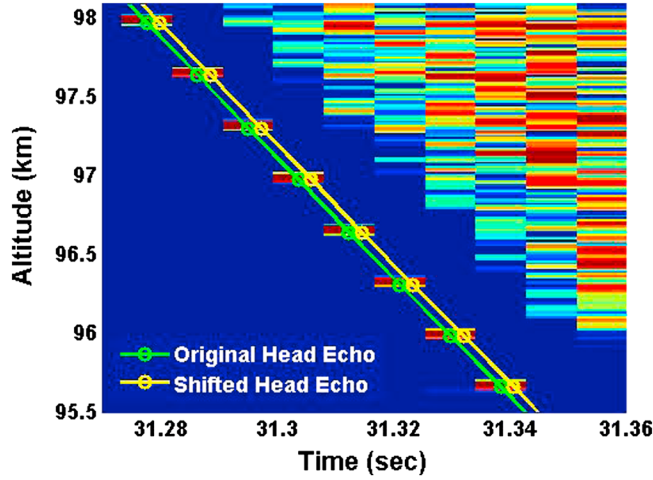
Figure 3. Example of a head echo before (green) and after (yellow) the necessary time shift due to the range-Doppler coupling. For this VHF case, the head echo needed to be shifted by 0.0022 s. Trail data example is from 9 January 2007.

highly collisional environment [*Greenhow and Neufeld*, 1955; *Dyrud et al.*, 2001; *Oppenheim et al.*, 2003b]. By making these assumptions, the ambipolar diffusion coefficient becomes a suitable approximation of the diffusion of the ions and electrons within the plasma. If the magnetic field influence is neglected, the coefficient can be described by equation (2) [*Chen*, 2006].

$$D_a = \frac{\mu_i D_e + \mu_e D_i}{\mu_i + \mu_e} \quad (2)$$

where μ is the mobility coefficient (equation (3)), D is the classical diffusion coefficient (equation (4)), and the subscripts denote ions or electrons.
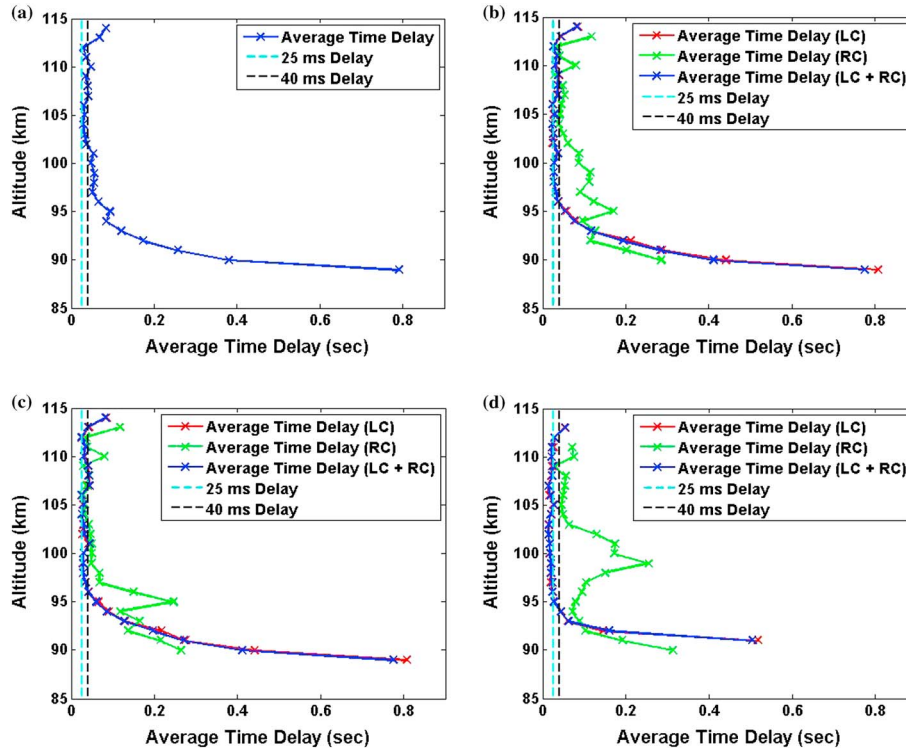

Figure 4. Time delays to the onset of turbulence within the nonspecular trails plotted verse altitude for (a) all trails and returns (b) delineated by signal return, (c) only VHF returns, and (d) only UHF returns. Dotted lines are also included to indicate where the time delays correspond to 25 and 40 ms in order to compare with previous studies.
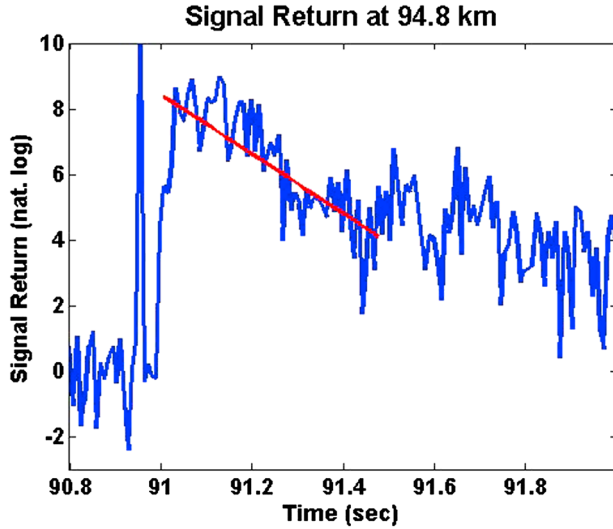
Figure 5. Signal return (blue) at altitude slice of 94.8 km from a trail detected on 2 January 2007 at VHF demonstrating the line fitting (red) to the signal for calculation of the diffusion coefficient.

$$\mu_j = \frac{q_j}{m_j v_{ji}} \tag{3}$$

$$D_j = \frac{K T_j}{m_j v_{ji}} \tag{4}$$

where q is the charge, m is the mass, v is the collision frequency between particles i and j , K is the Boltzmann constant, T is the temperature, and the subscripts denote individual i or j particles.

[13] However, the flux equations, as found in *Chen* [2006], including the magnetic field are not easily separated into one-dimensional equations. In this case, we are left with a more complicated process for arriving at an analytical solution for the ambipolar diffusion coefficient that is not as simply described as in equation (2). In the presence of a magnetic field, the diffusion and mobility coefficients are anisotropic. The electron flux will be greater than the ion flux in the parallel to the magnetic field direction, while the opposite is true in the perpendicular direction. As before, an electric field would be set up to aid the electron diffusion and ion diffusion in the perpendicular direction and parallel direction, respectively. However, in the case of boundary conditions being modeled as conducting plates, the perpendicular electric field can be short circuited by the escape of electrons along the magnetic field lines. This would reduce the negative charge produced by the imbalance of fluxes and result in non-ambipolar diffusion in the perpendicular direction even though the total diffusion would be ambipolar. In this case, the ions would then diffuse primarily perpendicular to the magnetic field lines, while the electrons would diffuse primarily along the magnetic field lines.

3.1. Extraction of Coefficient From Radar Signal

[14] In order to analyze the diffusion of nonspecular trails with radar, we used a relationship found between the decay of the radar signal and the radar wavelength. Many studies have suggested that, assuming a low electron density

($< 10^{12}$ electrons/cm) in the trail characterized by an exponential decay in signal return with time, the relationship between radar signal and wavelength can be described by

$$\tau = \frac{\lambda^2}{16 \times \pi^2 \times D_a} \tag{5}$$

where τ is the time decay constant and λ is the radar wavelength [*Greenhow and Neufeld*, 1955; *Hocking et al.*, 2000].

[15] Equation (5) has been used in numerous studies to extract ambipolar diffusion coefficients from radar-detected specular trails [*Weiss*, 1954; *Greenhow and Neufeld*, 1955; *Chilson et al.*, 1996; *Galligan et al.*, 2004]. These specular trail studies used the exponential decay in time of the SNR signal to calculate a time decay constant. This process begins by first plotting the trail's SNR against time for a given altitude and finding the time it takes for the SNR to return to $1/e$ of the initial peak. The natural log (nat. log) of the data is then fitted to a line between these two times, the initial peak of the trail and the time when the SNR drops to $1/e$ of the initial peak. Figure 5 provides an example of this data-fitting technique from a nonspecular trail detected on 2 January 2007 around 6 A.M. local time. These data correspond to a slice in altitude (across all times) at 94.8 km. Using the properties of nat. log and exponentials, the slope of this fitted line gives the time constant directly since the slope is simply the reciprocal of the time constant. Subsequently, equation (5) was then used to calculate the diffusion coefficient for each trail from these time decay constants.

3.2. Coefficients of Nonspecular Trails

[16] Using the process described in section 3.1 from previous works, we computed time constants from the slopes of fitted data. We then calculated the diffusion coefficients using equation (5) over the range of altitudes for each of the 152 nonspecular trails. An example of the calculation for a single trail detected on 18 November 2007 around 6 A.M. local time at VHF is provided in Figure 6.

[17] Similar to the turbulence onset analysis presented above, we rounded to the nearest altitude, breaking down the results for LC, RC, and total signal return, and averaged across all 152 trails. The averaged coefficient results were then plotted versus altitude, as shown in Figure 7a, in order to determine altitude trends and compare with previous theory [*Jones and Jones*, 1990] and meteor studies [*Galligan et al.*, 2004] for specular trails, which is included as the solid and dotted black lines, respectively, in Figure 7. *Jones and Jones* [1990] used theoretical predictions from ionic mobility theory to produce a numerical model, which agrees with laboratory and radio-meteor observations, for diffusion coefficient as a function of height. This simulation excluded chemical effects but did include the effects of multiple ion species diffusion in which the electron distribution remains approximately Gaussian. On the other hand, the model reported by *Galligan et al.* [2004] was derived from approximately 300,000 meteor detections between 1995 and 1999 at the Advanced Meteor Orbit Radar. This midlatitude radar primarily used a narrow 1.6° full width at half power beam at 26.2 MHz to detect meteors over a central site located in New Zealand. It must be noted that the authors did specify that the predictions are only appropriate between 85 and 105 km altitude since most of the meteors used for the
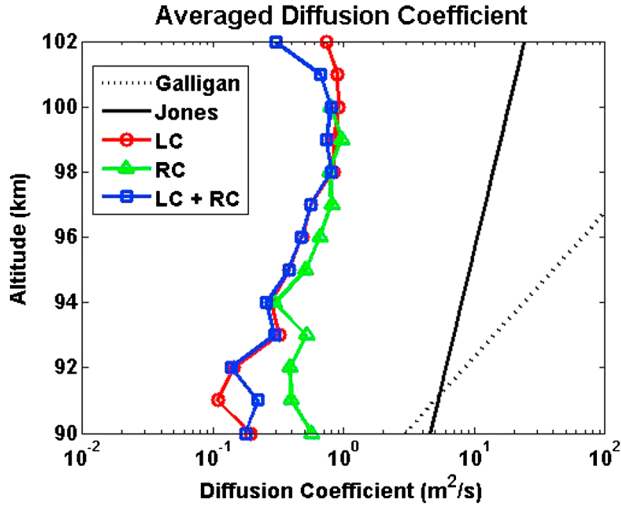
Figure 6. Example of diffusion coefficients calculated for a single trail detected on 18 November 2007 around 6 A.M. local time at VHF.

study fall between these altitudes. However, the simple averaging over all trails does not account for sparse trails and smaller time constants, which could possibly skew the results toward a higher diffusion coefficient average. In order to account for this biasing factor, we also weighted the average of the coefficients by the number of signal return points that

were greater than 20 dB and plotted these results as a function of altitude in Figure 7b. Additionally, we further categorized the trails by detection frequency and presented averaged coefficients for VHF and UHF in Figures 7c and 7d, respectively. We also included a 95% confidence bound based on the error in fitting a line to the data on all of the averaged coefficients plots. Notice that at a few of the higher and lower altitudes, the 95% confidence bounds become very large because of the scarcity of detected points.

[18] If we look at the averaged diffusion coefficient in Figure 7a, it is difficult to discern any pattern in the diffusion coefficient. The coefficient in this figure seems to remain relatively constant as a function of altitude. On the other hand, if we examine the weighted coefficients in Figure 7b, we begin to see a trend of increasing diffusion coefficient with increasing altitude between 95 and 110 km, which is also evident when we separate the results by frequency. These results indicate that at higher altitudes, the nonspecular trails are diffusing outward from the head echo source position faster than at lower altitudes, which agrees well with theory and with the results we found for a single 1998 nonspecular trail also detected by ALTAIR [*Yee and Close*, 2011]. This follows conventional knowledge that the neutral densities are smaller at higher altitudes, which would result in fewer collisions impeding the diffusion of nonspecular trails at higher altitudes. At altitudes below 95 km in Figures 7b and 7c, the calculated diffusion coefficients begin to increase again with decreasing altitude. This opposite trend might be
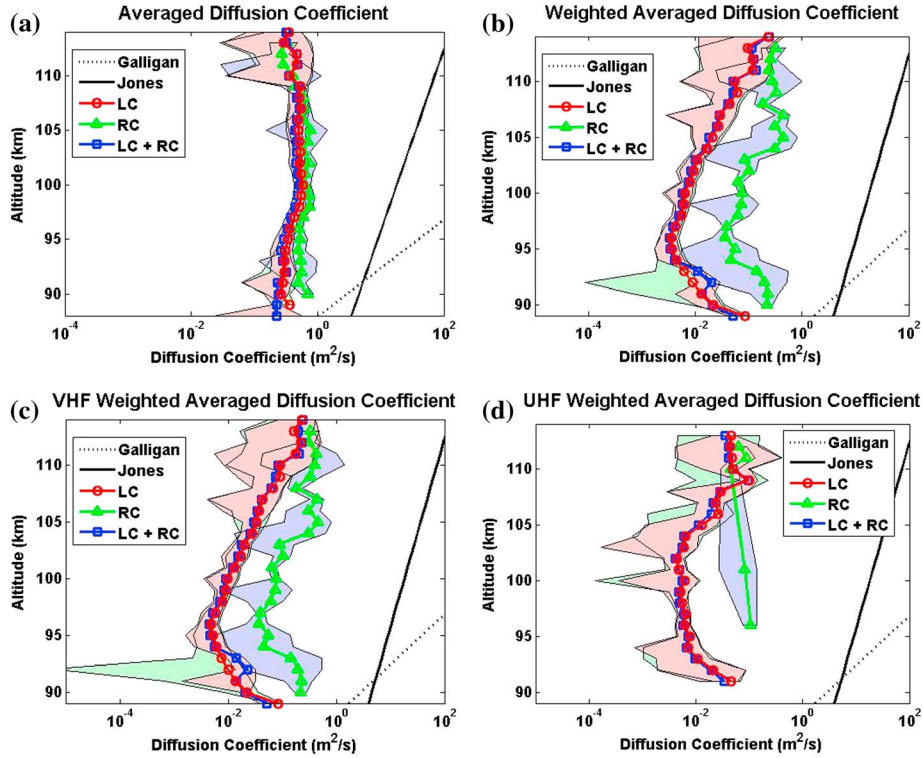

Figure 7. Diffusion coefficients (a) averaged and (b) number of points weighted average broken down for type of signal return. The coefficients are further broken down by type of frequency (c) VHF and (d) UHF. A theory study [*Jones and Jones*, 1990] and radar meteor study [*Galligan et al.*, 2004] of ambipolar diffusion coefficients for specular trails are also included in solid and dotted, respectively, black lines for comparison. All plots show a 95% confidence interval on the estimation of the averaged coefficients with green, blue, and red shading representing LC, RC, and total return, respectively.
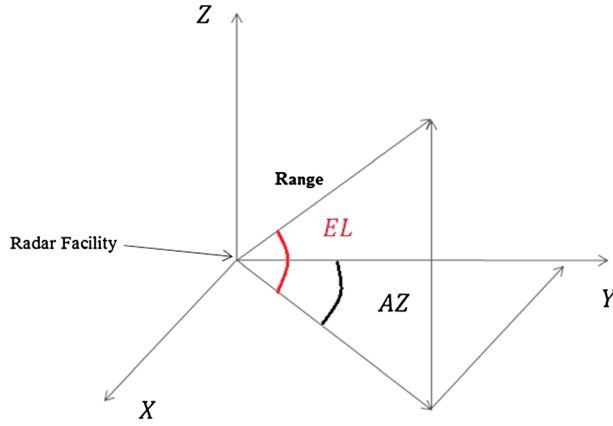
Figure 8. Geometry used to solve 3-D positions from monopulse angles.

explained by the scarcity in trail points during the averaging as indicated by larger confidence intervals at those altitudes. However, previous research [*Dyrud et al.*, 2001; *Ballinger et al.*, 2008] has suggested that this trend is actually a physical process driven by the dominance of recombination and collisions in the expansion process at lower altitudes. Additionally, both trends are consistent regardless of the polarization of the return with slight magnitude differences for the RC return, which may be due to the lack of return points sufficiently above the noise.

[19] While the general trend that we found in the ALTAIR data of increasing diffusion coefficient with increasing altitude is consistent with previous measurements, it must be noted as seen in Figure 7 that the magnitude of these coefficients do not agree with either the *Jones and Jones* [1990] theoretical predicted values or the *Galligan et al.* [2004] modeled values that were determined from specular trail ambipolar diffusion coefficients. In fact they predicted ambipolar coefficients that were 2–5 orders of magnitude greater than our calculated coefficients. This magnitude difference between previous studies and our calculated coefficients seems to be a common occurrence regardless of the breakdown or calculation method, and in fact is the case when we compare magnitudes of our calculated diffusion coefficients with meteor studies done at the 32.5 MHz SKiYMET radar [*Ballinger et al.*, 2008], the 31 MHz Nippon/Norway Svalbard Meteor Radar [*Hall et al.*, 2005], and the 35.25 MHz Thumba radar [*Kumar and Subrahmanyam*, 2012]. It should be noted that these studies disregarded the effects of the magnetic field on meteor diffusion since they found no geomagnetic effects with respect to enhancements in the diffusion, even though they did not examine the diffusion in each direction, perpendicular and parallel, relative to the magnetic field. In addition, these studies calculated ambipolar diffusion coefficients in a similar fashion to the process described above, but as mentioned before, all these previous works used specular trail detections which only span a single altitude range for a given parent meteor and arise from a different scattering mechanism (i.e., Fresnel scattering and Bragg scattering for specular and nonspecular trails, respectively), which may influence the results. We believe the different scattering mechanisms in combination with the different viewing

geometry, beam perpendicular to the magnetic field, and altitude span for nonspecular trails are the source of the differences in magnitude of diffusion coefficients. This could actually indicate that the nonspecular trail detections used in our analysis provide more information about the diffusive properties, including magnetic field effects, that need to be accounted for when calculating diffusion coefficients, thereby compelling an examination of the trail diffusion shapes over time.

4. Meteor Trail Diffusion Shape

4.1. Estimation of Trail Position Using Monopulse Angles

[20] ALTAIR's five horn receiving system permits a study of the 3-D evolution of meteor trail shape from the monopulse angles AZ and EL off of beam center. In order to calculate the 3-D positions of nonspecular trail particles, we used these monopulse angles of the nonspecular trails in combination with the fixed angles of ALTAIR. Using an Earth-fixed coordinate system originating at ALTAIR, as in Figure 8, we apply simple geometry to determine the positions from a combination of cosine and sine of the angles and the range to the target. The positions are found using equations (6), (7), and (8),

$$x = r \times \cos(\alpha_A + \alpha) \times \sin(\beta_A + \beta) \qquad (6)$$

$$y = r \times \cos(\alpha_A + \alpha) \times \cos(\beta_A + \beta) \qquad (7)$$

$$z = r \times \sin(\alpha_A + \alpha) \qquad (8)$$

where r is the range to the target, α_A and β_A are the set elevation and azimuth angles, respectively, of ALTAIR, and α and β are the offset elevation and azimuth angles, respectively, of the target. ALTAIR set elevation angle varied from 45° up to 83°, while the set azimuth angle varied from 35° to 360°.

[21] Using these equations, we calculated 3-D positions for each trail using the monopulse offset angles for each trail. Figure 9 shows an example of the detected 3-D positions changing with time for a head echo and nonspecular trail detected around 6 A.M. on 2 January 2007 for LC return at VHF when the angle between ALTAIR's beam and the magnetic field lines was approximately 93°. This particularly strong trail was detected across 13 km in altitude (91–104 km) and lasted nearly 3 s. Points color coded for LC return power in dB are plotted to represent the trail's offset from beam center (x-y) and altitude. The five images in Figure 9 show different instances of the trail's development. At 0.0348 s, only the head echo circled in red is visible. However, less than 1 s later, the head echo has moved several kilometers down in altitude and the meteor trail has begun to form in the wake of the head echo. As the head echo moves downward, the trail continues to develop until it appears to form a column of plasma with strong returns between altitudes of 94 and 98 km at 0.3391 s. After the head echo is no longer detected, the trail continues to diffuse outward until the signal return falls back to the noise level as evidenced at 1.0348 s when the higher altitudes no longer show trail detection. Notice that the projected beam size at 100 km and magnetic field lines are also included as the blue circle and black lines.
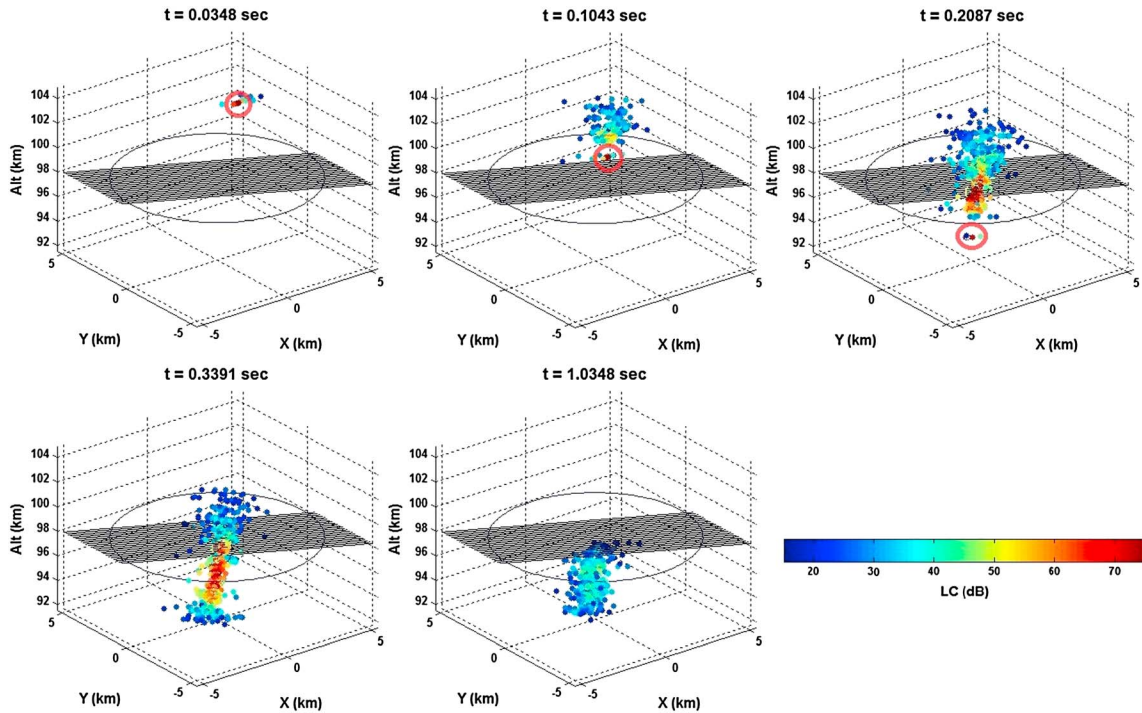
Figure 9. Three-dimensional trail evolution through time at 0.0348, 0.1043, 0.2087, 0.3391, and 1.0348 s with the head echo circled in red in the first several images when it is detected. The images are plotted with respect to distance from beam center in the *x-y* direction and altitude in kilometers and color coded for LC return in decibels. The magnetic field lines and a projected beam size at 100 km have also been included and are shown by the black lines and blue circles, respectively. The data points come from a trail detected on 2 January 2007 around 6 A.M. local time.

[22] Because the averaged diffusion coefficients' magnitude did not agree with the magnitude of ambipolar diffusion coefficients predicted by previous models, we examined the diffusion shape of the nonspecular trail with time in order to explore the assumptions inherent in ambipolar diffusion, namely that particles diffuse predominately in the direction parallel to the magnetic field. In order to study this diffusion, we first found the average *x-y* position of the head echo in the 2-D plane in order to establish a new coordinate system that was aligned parallel and perpendicular with the magnetic field in the *x* and *y* directions, respectively. An example of this new rotated coordinate frame is included in Figure 10,
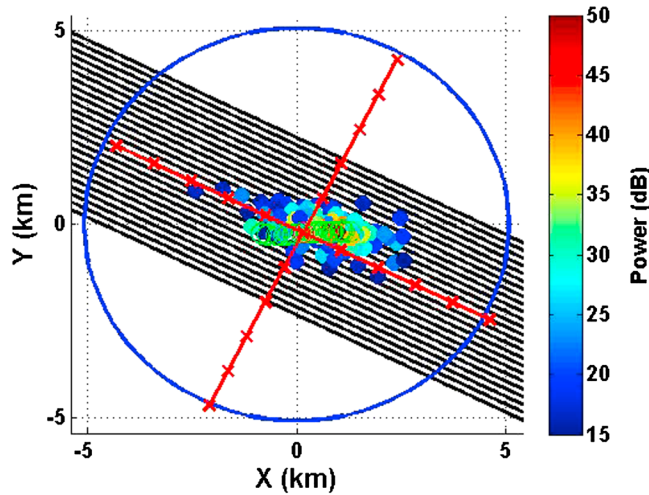

Figure 10. Trail's 2-D position detected on 2 January 2007 around 6 A.M. local time at 0.1043 s into detection. The head echo has been added as the green circles with the original and rotated center point being the red circle. The red lines with crosses are showing the new coordinate system rotated form the original *x-y* coordinate system that was used to calculate the variation of nonspecular trail points parallel and perpendicular to the magnetic field lines shown in black.
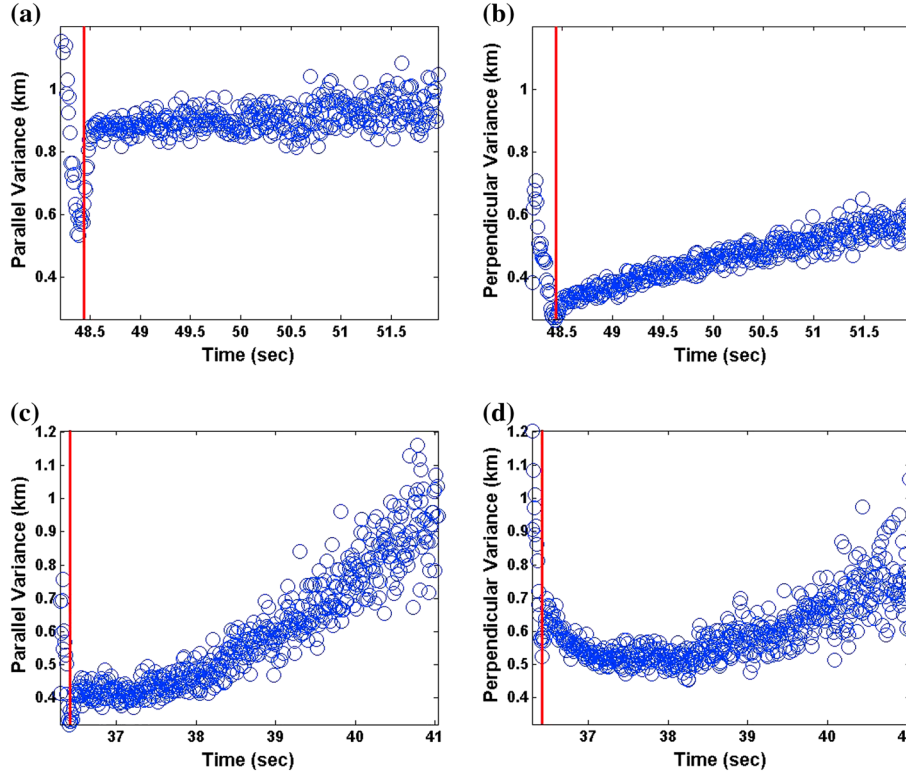
Figure 11. Examples of (a, c) parallel and (b, d) perpendicular variations from the magnetic field lines calculated over the nonspecular trail's detection time span. The red line in all four plots designate the time at which the head echo is no longer detected. Trail examples are from detections around 5 A.M. local time on (a, b) 6 January 2007 and (c, d) 5 January 2007.

where the 2-D plane with the x-y positions of the meteor trail described above at 0.1043 s is overlaid with the new coordinate system as red lines. Notice that the red lines are now aligned with the black magnetic field lines. The origin of the new coordinates is simply the average x-y position of the head echo shown as the red circle in the head echo path (green circles).

[23] At each time sample, we then calculated the average variation of detected points from the x and y axes, which corresponds to the perpendicular and parallel variations, respectively. We then fitted a line to these variation points with respect to time duration and examined the magnitude of the slopes scaled by the duration of the trail. This final magnitude of the slope for each direction gives an indication of how quickly the nonspecular trail is diffusing in the parallel or perpendicular to the magnetic field direction relative to the head echo's central point, with larger values showing quicker diffusion for a given period of time. The standard deviations of the first and last five average variations were also calculated for each trail for both the parallel and perpendicular direction. These parameters, like the scaled slopes, give additional information about the diffusion parallel and perpendicular to the magnetic field. More specifically, the changes in the standard deviation of a nonspecular trail in each direction will show how much the trail has diffused outward from the head echo path in either direction during the detection time frame. Combined, these two parameters provide a good indication of how the trail is diffusing in time.

4.2. Diffusion Perpendicular and Parallel to the Magnetic Field

[24] The processes described above were applied to our data set to produce the average variations examples in Figure 11, after removing the heads. These figures show the deviations perpendicular and parallel to the magnetic field lines over the time duration of the nonspecular trail.

[25] As can be seen in Figure 11, the beginning portions (i.e., sections to the left of the red line that indicates where the head echo is no longer detected) seem to be wildly varying in comparison to the rest of the trail. It could be that these portions, even though we removed the main head echo detection, may still have some residual influence from head echo fragmentations that could not be fully removed since they are detected at times between the initial head echo detection and the full development of the nonspecular trail [*Mathews et al.*, 2010]. However, a more detailed analysis of one of these fragmentation events and its corresponding trail revealed that these fragmentation influences do not account for all of the variation. Another suggestion could be that the neutral winds suddenly changed directions and caused the meteor trail to be "dragged" in the opposite direction of the original diffusion [*Oppenheim et al.*, 2009], thereby causing an inflection point in the average variation of the meteor trail. However, we believe that the main factor for these large varying portions are due to detection of the meteor plasma in the initial stages of turbulence after the instabilities have grown large enough. In this stage
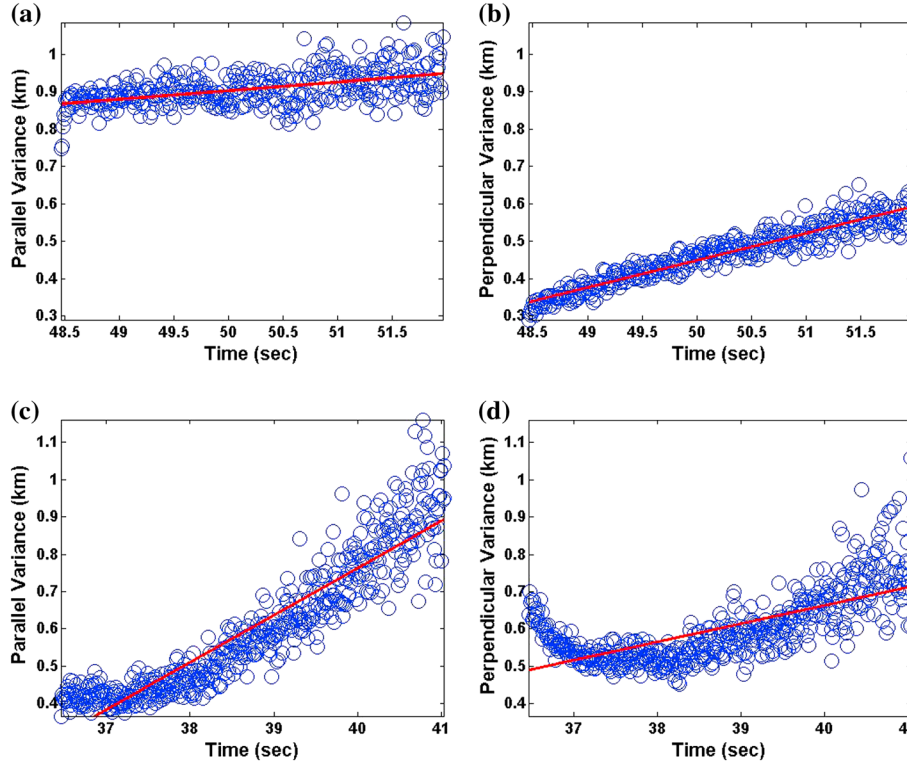
Figure 12. Examples of (a, c) parallel and (b, d) perpendicular variations from the magnetic field lines calculated over the nonspecular trail's detection time span with the noisy beginning region removed. A red line is fitted to the data for further analysis of the change in position with time. These examples are from the same trails as in Figure 11 and thus can be compared directly to see the trail with and without noisy region at the beginning. Trail examples are from detections around 5 A.M. local time on (a, b) 6 January 2007 and (c, d) 5 January 2007. Notice that the beginning variation does not vary linearly with the later variations. We believe this could be due to lingering effects from detection of density irregularities within the plasma before they have fully aligned with the magnetic field at the lower altitudes of the given trail.

of trail development, we could be detecting the density irregularities within the plasma as they are initially forming and attempting to align with the magnetic field. These ideas warrant further investigation and will be undertaken in future work. We therefore decided to only examine the later portion of the nonspecular trails to avoid skewing the average variance of points due to these possible biases. Examples of these trails without the large variations are shown in Figure 12 for the same trails as Figure 11. In these cases, we see the variation spread increase in time which shows the nonspecular trail is diffusing outward from the path of the head echo; this is a common feature for most of the trails. It should be noted that there is a portion at the beginning of the average variance that sometimes does not follow with the linear variation found in the later portion of the nonspecular trails, as can be seen in Figures 12c and 12d. We believe this is also a result of lingering effects from detection of density irregularities within the plasma before they have fully aligned with the magnetic field at the lower altitudes of a given trail. This is possible because the turbulence onset and development of field-aligned irregularities will occur at a trail's lower altitudes later in time since it is a function of when the meteoroid passes these regions.

[26] Once the left side of the average variations was removed, we found weighted slopes for the average variance as described above. These weighted slopes are shown in

Figure 13 for parallel (Figure 13a) and perpendicular (Figure 13b) directions with respect to the magnetic field. In addition to the slopes (blue points), we also included the error on the fits for the slopes (red lines). The trails were ordered based on perpendicular slope fit errors with the smallest error starting on the left. Parallel fits were ordered corresponding to the perpendicular order such that an easy comparison could be made between the two plots. In order to achieve a better examination of the values with small fit errors for comparison, zoomed views for the parallel (Figure 13c) and perpendicular (Figure 13d) direction were also provided. In examining the slopes of the fits, we see that the fitted values can become quite noisy as the error range increases, which is most likely due to a trail with variations that are not increasing or decreasing linearly with time, as in Figure 12d. However, for the slope values where the fits have lower error, we can see that calculations show that the parallel and perpendicular directions have similar slope magnitudes for the corresponding trails. This result indicates that the trails are moving equivalent distances in the parallel and perpendicular directions with respect to the magnetic field for most trails.

[27] As can be seen in Figures 12c and 12d, the data points are often hard to fit linearly. In order to explore the variations further, we also examined the spread of each nonspecular trail as the trail evolved with time. As described above, we
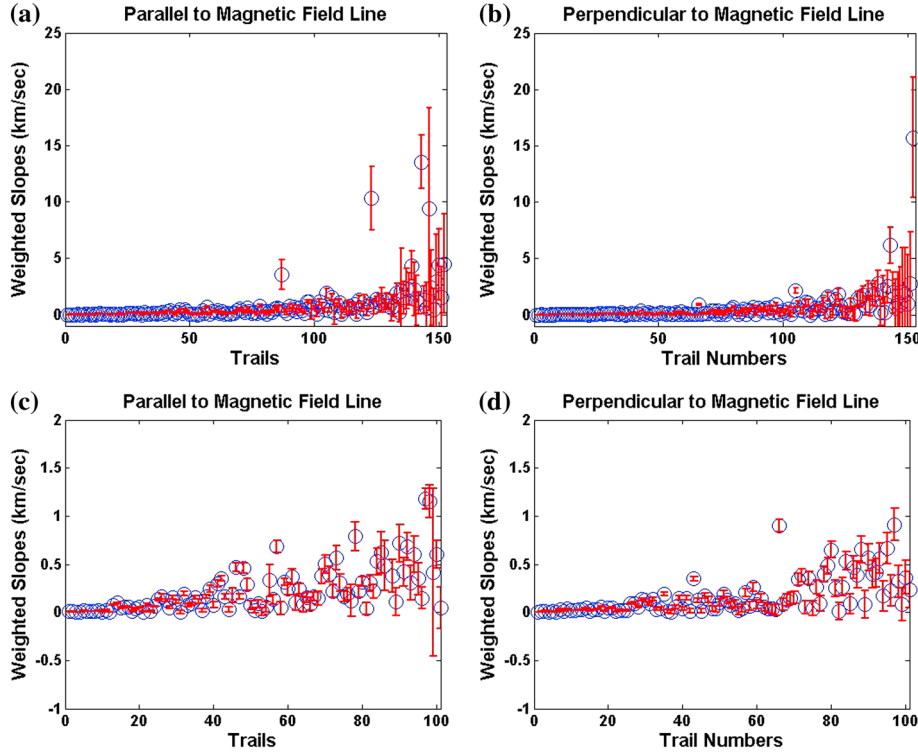
Figure 13. Slopes weighted for the duration of time from the fit of the average variation of points with time for the (a) parallel and (b) perpendicular to the magnetic field lines directions for all 152 trails. The red lines represent the error for the given fitted slope for each trail. Zoomed views are also shown for (c) parallel and (d) perpendicular in order to better view the smaller values on the left side.

calculated the standard deviation at the beginning and end of the trail's time period. We then subtracted the beginning standard deviation from the end in order to show the difference in the change in standard deviation between the parallel (blue circles) and perpendicular (red triangles) to the magnetic field lines as plotted in Figure 14. The results are organized based on the difference between the parallel and perpendicular directions. The largest differences are toward the edges with perpendicular being greater to the left of the vertical black line and parallel to the right.

[28] In total, 50 trails had larger changes in standard deviation in the perpendicular direction versus 102 trails had greater values for the parallel direction. Additionally, the center portion, trails 25 to 100, of Figure 14 indicates that a large number of trails had diffusion spread magnitudes that were comparable between both directions.

[29] For the approximately 50 trails that exhibited greater diffusion in the perpendicular direction, we examined the head echo velocities, maximum head echo SNR return, nonspecular trail altitudes, nonspecular trail durations, detection frequency, and angle between the radar beam and magnetic field to investigate any potential correlations among these quantities. However, the only comparison that seemed to have a correlation with the diffusion direction was the nonspecular trail durations, which are shown in Figure 15. The blue circles indicate the duration of the nonspecular trail in seconds and has been organized in the same manner that the change in standard deviation was organized. If we compare Figures 14 and 15, we can see that in the regions where a particular diffusion direction (either perpendicular

or parallel) dominates, the time duration of the nonspecular trail is relatively short, whereas when the perpendicular and parallel diffusion rates are similar, the time duration is relatively long. Because shorter trail detection times indicate
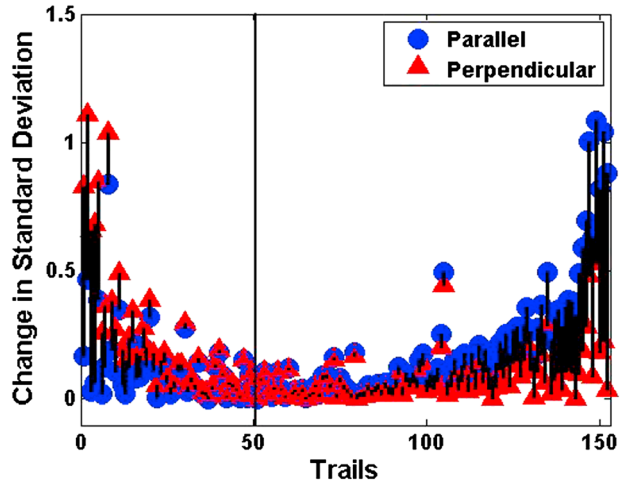

Figure 14. Difference between the standard deviation from the end and beginning of the nonspecular trail variations for all 152 trails. The results have been organized such that values to the left of the black line indicate cases where the perpendicular value is larger than the parallel value, whereas values to the right are the opposite. Blue circles correspond to parallel direction differences, while red triangles refer to perpendicular direction differences.
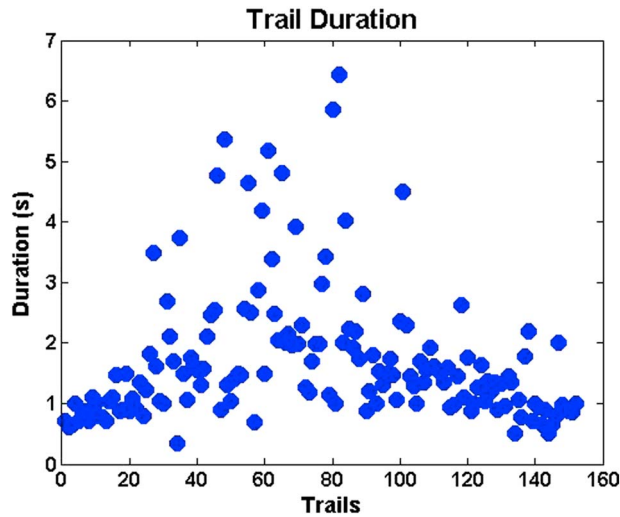
Figure 15. Trail durations in blue circles for all 152 nonspecular trails organized in similar fashion to Figure 14. Notice large differences between the perpendicular and parallel change in standard deviation correlate with shorter duration trails.

a weaker nonspecular trail, other ambient conditions, especially neutral winds or ambient electric fields, may become more prominent in the diffusion direction of these trails than in stronger, longer duration trails. This explanation of neutral wind or electric field effects has not fully been explored with this data and will be explored in future analysis.

[30] Regardless, the combination of the two results, weighted slopes and change in standard deviation, indicates that nearly 50% of the trails we analyzed spread on the same order of magnitude in the perpendicular direction as in the parallel direction, with an additional 20% spreading more in the perpendicular direction, though more analysis of whether this disparity between directions is truly trail diffusion driven or ambient conditions driven needs to be done on these shorter duration trails. This result from the change in standard deviation in Figure 14 coincides with the result from the examination of the fitted slopes in that both results show that the nonspecular trail diffusion has generally equal contributions from the diffusion in parallel and perpendicular to the magnetic field direction. This contradicts the theory of fully ambipolar diffusion in the presence of a magnetic field in this region of the ionosphere since the electrons, which produce the signal return detected, should primarily diffuse in the parallel direction.

[31] These results agree with the results of nonspecular trail simulations reported by *Dyrud et al.* [2001], which showed that the perpendicular direction could be enhanced by anomalous cross-field diffusion to the point where it was on the same order of magnitude as the parallel direction. From his simulations, density gradients were shown to drive gradient drift instabilities, which then developed into waves with perturbed electric fields. It is suggested that these waves drive the anomalous cross-field diffusion that allows the electrons to diffuse at rates different from the ions in the perpendicular to the magnetic field direction, while also maintaining the ambipolar diffusion rates seen by previous specular trail studies. It is very likely that the diffusion enhancements seen in our measurements for the perpendicular

direction are due to this anomalous cross-field diffusion suggested by *Dyrud et al.* [2001]. Additionally, *Dyrud et al.* [2001] noted that lower density trails (i.e., weakly detected trails) could have much lower anomalous diffusion if there were no neutral winds to produce the large electric field perturbations. This could be an explanation of why the shorter trails exhibited larger differences in their change in standard deviations between each direction, with the inhibited perpendicular diffusion trails being detected at times with low or no neutral winds and large neutral winds for the enhanced perpendicular diffusion trails.

5. Conclusion

[32] We analyzed the turbulence onset times, diffusion coefficients, and average variation of the trail with respect to the magnetic field for 152 nonspecular trails detected by ALTAIR in 2007. Calculated turbulence onset times agree with model predictions of nonspecular trail development and evolution. For the most part, calculated onset times fall below 40 ms with the exception being the sharp increase in onset times with altitude below 95 km. RC returns, especially for UHF trails, show some interesting patterns that could be linked to the detection dependence on return type and frequency, which definitely warrant further investigation. Diffusion coefficients were also calculated from the nonspecular trail returns by using methods that examine the decay in the signal return with time. Although simple averaging across all 152 nonspecular trails produced no apparent pattern in the diffusion coefficients, the weighted average of diffusion coefficients yielded the expected pattern of increasing diffusion coefficient with increasing altitude for the middle range of altitudes; the expected opposite trend appeared at the lower altitudes where recombination and collisions become the dominant factors. However, in comparison to specular trail ambipolar diffusion coefficients, we found that the calculated coefficients are orders of magnitude smaller than expected. This may be attributed to a combination of the processes leading to different scattering mechanisms and different viewing geometry between the radar beam and the magnetic field lines, which could allow for a better detection in nonspecular trails of the anomalous diffusion predicted by Dyrud in addition to the ambipolar diffusion detected in specular trail studies. The change in average variation of points with respect to the magnetic field was examined and shown to be fairly similar between the parallel and perpendicular directions. In conjunction with the fitted slopes, the examination of the change in spread of the trails further showed that the parallel and perpendicular diffusion rates are comparatively similar. For the trails that differed greatly between the two directions, we suggested that this could possibly be a result of ambient conditions more prominently affecting the diffusion direction or lower anomalous diffusion rates because of the shorter, weaker trails. Future exploration of this hypothesis and its effects could involve comparing the effects of neutral wind measurements on the shorter and longer duration trails. However, with the calculated coefficients being on different orders of magnitude from previous studies and the change in shape demonstrating equivalent diffusion rates in the directions perpendicular and parallel to magnetic field, we have shown that the ambipolar diffusion description does not encompass

all of the diffusion processes that can be seen in nonspecular trails detections, thereby confirming results found by *Dyrud et al.* [2001] in nonspecular trail simulations. Therefore, it is our conclusion that we need a new description and calculation method of the diffusion of meteor trails that not only includes the random movement, recombination, and collisions of plasma particles but also the effects of the background ionosphere, such as Earth's magnetic field and any external electric field, and any enhancements due to anomalous cross-field diffusion.

References

Ballinger, A. P., P. B. Chilson, R. D. Palmer, and N. J. Mitchell (2008), On the validity of the ambipolar diffusion assumption in the polar mesopause region, *Ann. Geophys.*, *26*, 3439–3443, doi:10.5194/angeo-26-3439-2008.

Chau, J., R. Woodman, and F. Galindo (2007), Sporadic meteor sources as observed by the Jicamarca high-power large-aperture VHF radar, *J. Icarus*, *188*, 162–174, doi:10.1016/j.icarus/2006.11.006.

Chen, F. F. (2006), Diffusion and resistivity, in *Introduction to Plasma Physics and Controlled Fusion*, Plasma Physics, vol. 1, 2nd ed., pp. 155–198, Springer, New York, NY.

Chilson, P. B., P. Czechowsky, and G. Schmidt (1996), A comparison of ambipolar diffusion coefficients in meteor trains using VHF radar and UV lidar, *Geophys. Res. Lett.*, *23*, 2745–2748, doi:10.1029/96GL02577.

Close, S., M. Oppenheim, S. Hunt, and L. Dyrud (2002), Scattering characteristics of high-resolution meteor head echoes detected at multiple frequencies, *J. Geophys. Res.*, *107*(A10), 1295, doi:10.1029/2002JA009253.

Close, S., T. Hamlin, M. Oppenheim, L. Cox, and P. Colestock (2008), Dependence of radar signal strength on frequency and aspect angle of nonspecular meteor trails, *J. Geophys. Res.*, *113*, A06203, doi:10.1029/2007JA012647.

Close, S., P. Colestock, M. Kelley, L. Cox, and N. Lee (2010), Electromagnetic pulses from hypervelocity impacts, *J. Geophys. Res.*, *115*, A12328, doi:10.1029/2010JA015921.

Close, S., M. Kelley, L. Vertatschitsch, M. Oppenheim, and J. Yee (2011), Polarization and scattering of a long-duration meteor trail, *J. Geophys. Res.*, *116*, A01309, doi:10.1029/2010JA015968.

Dyrud, L. P., M. M. Oppenheim, and A. F. vom Endt (2001), The anomalous diffusion of meteor trails, *Geophys. Res. Lett.*, *28*, 2775–2778, doi:10.1029/2000GL012749.

Dyrud, L. P., M. M. Oppenheim, S. Close, and S. Hunt (2002), Interpretation of non-specular radar meteor trails, *Geophys. Res. Lett.*, *29*(21), 2012, doi:10.1029/2002GL015953.

Dyrud, L. P., L. Ray, M. Oppenheim, S. Close, and K. Denney (2005), Modeling high-power large-aperture radar meteor trails, *J. Atmos. Sol. Terr. Phys.*, *67*, 1171–1177, doi:10.1016/j.jastp.2005.06.016.

Dyrud, L. P., E. Kudeki, and M. M. Oppenheim (2007), Modeling long duration meteor trails, *J. Geophys. Res.*, *112*, A12307, doi:10.1029/2007JA012692.

Galligan, D. P., G. E. Thomas, and W. J. Baggaley (2004), On the relationship between meteor height and ambipolar diffusion, *J. Atmos. Sol. Terr. Phys.*, *66*, 899–906, doi:10.1016/j.jastp.2004.03.002.

Greenhow, J. S., and E. L. Neufeld (1955), The diffusion of ionized meteor trails in the upper atmosphere, *J. Atmos. Terr. Phys.*, *6*, 133–140, doi:10.1016/0021-9169(55)90020-9.

Hall, C. M., T. Aso, M. Tsutsumi, S. Nozawa, A. H. Manson, and C. E. Meek (2005), Testing the hypothesis of the influence of neutral turbulence on the deduction of ambipolar diffusivities from meteor trail expansion, *Ann. Geophys.*, *23*, 1071–1073, doi:10.5194/angeo-23-1071-2005.

Heritage, J. L., W. J. Fay, and E. D. Bowen (1962), Evidence that meteor trails produce a field-aligned scatter signal at VHF, *J. Geophys. Res.*, *67*, 953–964, doi:10.1029/JZ067i003p00953.

Hocking, W. K., B. Fuller, and B. Vandepeer (2000), Real-time determination of meteor-related parameters utilizing modern digital technology, *J. Atmos. Sol. Terr. Phys.*, *63*, 155–167, doi:10.1016/S1364-6826(00)00138-3.

Jones, W., and J. Jones (1990), Ionic diffusion in meteor trains, *J. Atmos. Terr. Phys.*, *52*, 185–191, doi:10.1016/0021-9169(90)90122-4.

Kumar, K. K., and K. V. Subrahmanyam (2012), A discussion on the assumption of ambipolar diffusion of meteor trails in the Earth's upper atmosphere, *Mon. Not. R. Astron. Soc.*, *425*, L1–L5, doi:10.1111/j.1745-3933.2012.01279.x.

Lee, N., et al. (2012), Measurements of freely-expanding plasma from hyper-velocity impacts, *Int. J. Impact Eng.*, *44*, 40–49, doi:10.1016/j.ijimpeng.2012.01.002.

Mathews, J. D., S. J. Briczinski, A. Malhotra, and J. Cross (2010), Extensive meteoroid fragmentation in V/UHF radar meteor observations at Arecibo Observatory, *Geophys. Res. Lett.*, *37*, L04103, doi:10.1029/2009GL041967.

Oppenheim, M. M., A. F. vom Endt, and L. P. Dyrud (2000), Electrodynamics of meteor trail evolution in the equatorial E-region ionosphere, *Geophys. Res. Lett.*, *27*, 3173–3176, doi:10.1029/1999GL000013.

Oppenheim, M. M., L. P. Dyrud, and L. Ray (2003a), Plasma instabilities in meteor trails: Linear theory, *J. Geophys. Res.*, *108*(A2), 1063, doi:10.1029/2002JA009548.

Oppenheim, M. M., L. P. Dyrud, and A. F. vom Endt (2003b), Plasma insta-bilities in meteor trails: 2-D simulation studies, *J. Geophys. Res.*, *108*(A2), 1064, doi:10.1029/2002JA009549.

Oppenheim, M. M., G. Sugar, N. O. Slowey, E. Bass, J. Chau, and S. Close (2009), Remote sensing lower thermosphere wind profiles using non-specular meteor echoes, *Geophys. Res. Lett.*, *36*, L09817, doi:10.1029/2009GL037353.

Sugar, G. R. (1964), Radio propagation by reflection from meteor trails, *Proc. IEEE*, *52*, 116–136, doi:10.1109/PROC.1964.2801.

Weiss, A. A. (1954), Diffusion coefficients from the rate of decay of meteor trails, *Aust. J. Phys.*, *8*, 279–288, doi:10.1071/PH550279.

Yee, J., and S. Close (2011), Diffusion of plasmas from ablating meteoroids in the ionosphere, paper presented at Proceedings of the 3rd AIAA Atmospheric and Space Environment, American Institute of Aeronautics and Astronautics, Honolulu, Hawaii.